ACS APPLIED MATERIALS & INTERFACES

Research Article

www.acsami.org

Synthesis, Characterization, and Sunlight Mediated Photocatalytic Activity of CuO Coated ZnO for the Removal of Nitrophenols

M. Tariq Qamar,[†,‡] M. Aslam,[†] Iqbal M. I. Ismail,[†,‡] Numan Salah,[§] and A. Hameed*[,†,∥]

[†]Centre of Excellence in Environmental Studies (CEES), [‡]Chemistry Department, Faculty of Science, and [§]Centre of Nanotechnology, King Abdulaziz University, Jeddah 21589, Kingdom of Saudi Arabia

[∥]National Centre for Physics, Quaid-e-Azam University, Islamabad 44000, Pakistan

Supporting Information

ABSTRACT: CuO@ZnO core−shell catalysts, coated by varying the CuO layer density ranging from 0.5% to 10%, were synthesized with the aim to enhance the photocatalytic activity of ZnO in sunlight and control its photocorrosion. Initially, the Cu^{2+} ions were impregnated on presynthesized ZnO by wet impregnation and finally converted to CuO layers by calcination. The optical and structural characterization of the synthesized powders was performed by DRS, PL, Raman spectroscopy, and XRD analysis, respectively. The homogeneity of the coated layers was explored by FESEM. The photocatalytic activity of CuO coated ZnO was investigated for the degradation of mononitrophenols (2-, 3-, and 4-nitrophenol) and dinitrophenols (2,4-, 2,5-, and 2,6-dinitrophenol) in the exposure of the complete spectrum and visible region (420−800 nm) of sunlight. The effect of the increasing density coated layers of CuO on photocatalytic activity was evaluated for the degradation of 4-NP. Compared to pristine ZnO, a substantial increase in the degradation/mineralization ability was observable for the catalysts coated with 0.5% and 1% CuO, whereas a detrimental effect was noticed for higher coating density. Prior to photocatalytic studies, as evaluated by cyclic voltammetry (CV), compared to pure ZnO, a significant suppression of photocorrosion was noticed, under illumination, for catalysts coated with lower CuO coating. The progress of the photocatalytic degradation process was monitored by HPLC while the mineralization ability of the synthesized catalysts was estimated by TOC. The estimation of the released ions and their further interaction with the excited states and the reactive oxygen was monitored by ion chromatography (IC).

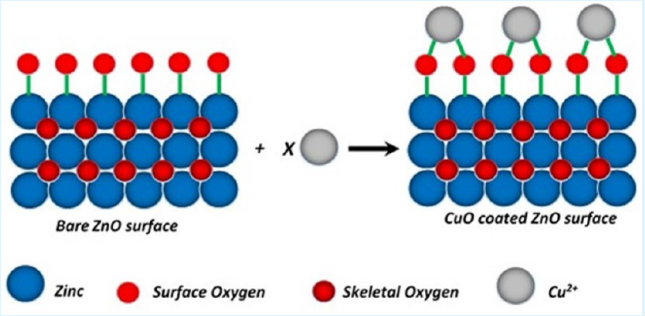

KEYWORDS: *sunlight photocatalysis, CuO coated ZnO, mononitrophenols, dinitrophenols*

1. INTRODUCTION

In the last few decades, advanced oxidation processes have been successfully used for the mineralization of harmful pollutants.[1−5] Photocatalysis, a protuberant off-shoot of advanced oxidation processes, has emerged as one of the most efficient methods for the complete mineralization of toxic organic pollutants.[2,3,6] The use of low-cost resources such as semiconductor materials, water, and light photons for the generation of reactive oxygen species (ROS) further authenticates its efficacy and economic viability.[1,7−10] In aqueous photocatalytic processes, the generation of ROS is primarily based on the light source of optimum energy for bandgap excitation. The majority of the research work on photocatalysis, available in the literature, is based on the use of artificial light sources. In our opinion, the use of costly light sources that convert electrical energy to photons not only is an impediment in the widespread commercial utilization of photocatalysis but also limits it for academic purposes only. We also believe that photocatalysis can achieve its utmost effectiveness with the use of inexpensive and ever renewable excitation/light sources. Sunlight is the most appropriate choice in this regard; however, it requires the development of photocatalysts capable of utilizing the major portion of sunlight with optimum activity. Two approaches are prevalent in this regard that include either developing new sunlight responsive photocatalysts or modifying the existing active catalysts for better sunlight response and photocatalytic activity.

A number of well-known semiconductors, such as TiO_2, ZnO, Bi_2O_3, WO_3, V_2O_5, SnO_2, Fe_2O_3, CdS, etc., have been studied as photocatalysts.[1,11−16] Among the aforementioned active photocatalysts, TiO_2 is the most widely studied for photocatalytic environmental remediation, whereas ZnO, with comparably broader absorption cross section, is regarded as the suitable alternative of TiO_2. Under sunlight illumination, ZnO furnishes better activity compared to TiO_2, as it absorbs a large fraction of the UV spectrum while additional visible light quanta, however, are disregarded due to photodissolution or photocorrosion. In our preceding studies, we have successfully

Received: February 9, 2015
Accepted: April 7, 2015
Published: April 7, 2015

DOI: 10.1021/acsami.5b01273
ACS Appl. Mater. Interfaces 2015, 7, 8757−8769

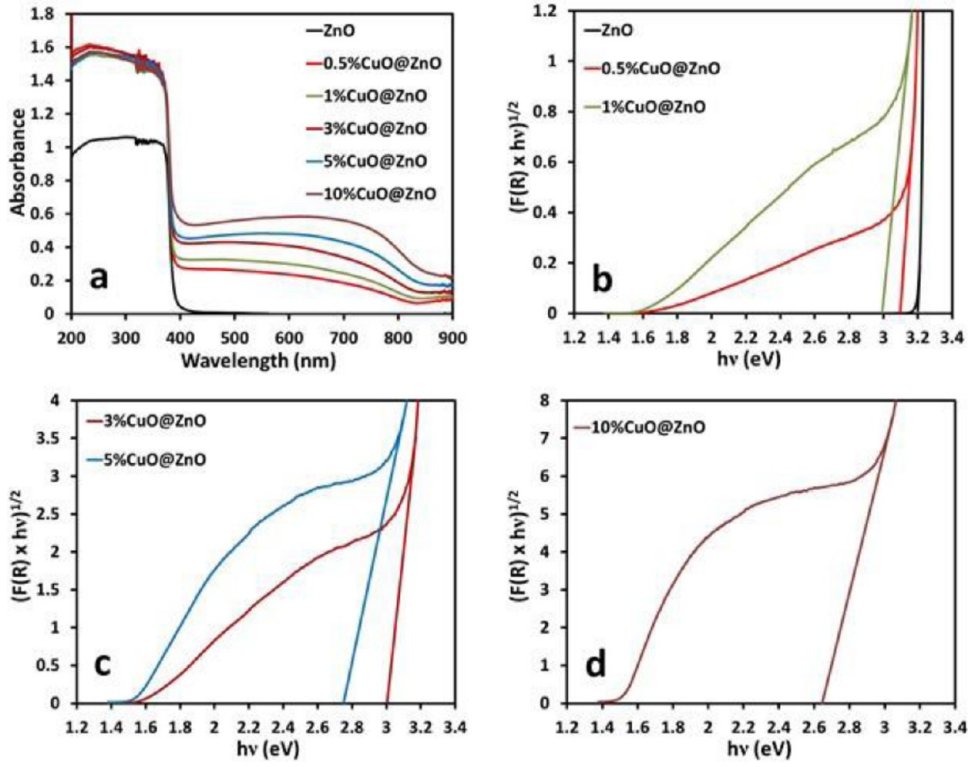

Figure 1. (a) Comparison of the solid-state absorption spectra of pure and *x*% CuO coated ZnO (*x* = 0.5, 1%, 3%, 5%, and 10%). (b–d) Graphical evaluation of the bandgaps of pure and CuO@ZnO powders.

demonstrated that the photocatalytic activity of ZnO can be enhanced in sunlight and the issue of photocorrosion can be addressed effectively by implanting a suitable surface trap for the efficient engagement of charge carries responsible for photocorrosion under illumination.[17−20]

Among toxic organic pollutants, the complete removal of nitrophenols, because of their toxic and carcinogenic health hazards, has been of major concern for decades.[19,21,22] Mono- and dinitrophenols, especially 2-nitrophenol, 4-nitrophenol, and 2,4-dinitrophenol, owing to their solubility, structural properties, resonance imparted chemical stability, and ability to transform into more toxic secondary pollutants, are the most difficult to remove by traditional wastewater treatment techniques.[23,24] The number of articles discussing the photocatalytic degradation of nitrophenols, in detail, are limited.[17,18,25]

In the current study, with a view to enhance the photocatalytic activity and suppress the photocorrosion of ZnO under sunlight exposure, the surface of ZnO was modified by coating it with CuO to form CuO@ZnO core−shell catalysts. A user-friendly approach was adopted for the synthesis of coated photocatalysts. The effect of increasing CuO layers density on photocatalytic activity under sunlight exposure was optimized for the removal of 4-NP. The optimized CuO layer density was further tested for the degradation of mononitrophenol (2-NP, 3-NP, and 4-NP) and dinitrophenol (2,4-DNP, 2,5-DNP, and 2,6-DNP) isomers under exposure of the complete spectrum as well as the visible region (420−800 nm) of sunlight.

2. EXPERIMENTAL DETAILS

CuO coated ZnO photocatalysts were synthesized by impregnating Cu^{2+} ions on the presynthesized ZnO. The synthesis of ZnO was carried out by the slow hydrolysis of zinc acetate using 0.1 M KOH. The detailed synthesis of ZnO is outlined in our previous communications.[18,19] The coated samples loaded with 0.5%, 1%, 3%, 5% and 10% of CuO with respect to the weight of ZnO were synthesized. The stoichiometry of the catalysts was adjusted on the basis of the amount of Cu^{2+}. In a typical synthesis, for 0.5% CuO coated ZnO, 0.00542g of $Cu(NO_3)_2.9H_2O$ (Sigma-Aldrich, 99.99%), containing 0.5% Cu^{2+} ions with respect to the weight of ZnO, was dissolved in 50 mL of deionized water. The precisely weighed amount of ZnO (10g) was added to the Cu^{2+} solution. The slurry was aged overnight under stirring for maximum adsorption of Cu^{2+} ion at the surface of ZnO. The excess water was removed by heating at 120 °C while the nitrates were decomposed at an elevated temperature of 250 °C that resulted in the impregnation of Cu^{2+} ions at the surface of ZnO with partial oxidation. For complete conversion of impregnated Cu^{2+} ions, the dried powder was calcined at 500 °C for 4 h in air with the heating rate of 10 °C per min.

The solid-state absorption and diffuse reflectance spectra (DRS) of the synthesized CuO coated ZnO photocatalysts were acquired by PerkinElmer UV−visible diffuse reflectance spectrophotometer in 190−900 nm range. The %R data was subjected to Kubelka−Munk transformation, F(R), for the evaluation of the absorption edges of the synthesized powders by plotting $(F(R) \times h\upsilon)^{1/2}$ versus $h\upsilon$ (eV). The photoluminescence (PL) emission spectra of the CuO coated ZnO powders were recorded by a fluorescence spectro-fluorophotometer, RF-5301 PC, Shimadzu, Japan at an excitation wavelength of 325 nm while the fluorescence emissions were recorded in the range of 350 to 650 nm. A DXR Raman Microscope, Thermo Scientific, USA, equipped with 532 nm laser as the excitation source at 6 mW power measured the Raman shifts. The powder XRD patterns of bare and Cu^{2+} impregnated ZnO powders were recorded by Xpert X-ray powder diffractometer (Philips PW1398) equipped with Cu Kα radiation source, from 20° to 80° (2θ) with a step time of 3 s and step size of 0.05°. Scherer's equation was applied on main reflections to evaluate the crystallite size of various phases. The changes in the morphology of ZnO base and the surface presence of Cu^{2+} species

DOI: 10.1021/acsami.5b01273
ACS Appl. Mater. Interfaces 2015, 7, 8757−8769

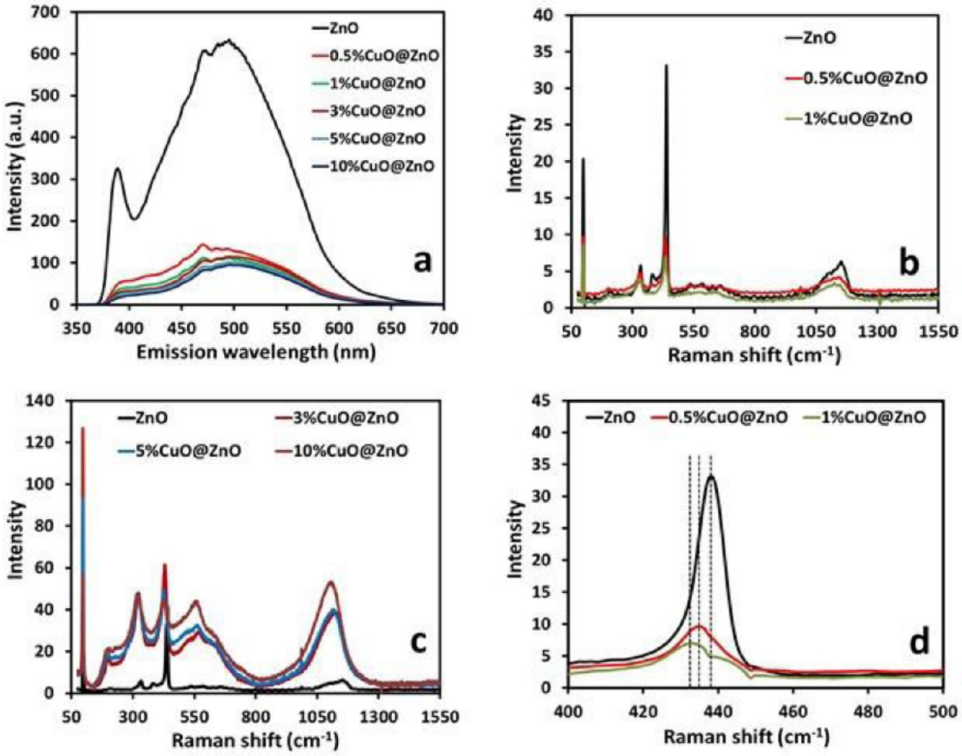

Figure 2. Comparison of (a) PL spectra of pure and CuO coated ZnO. (b) Raman spectra of ZnO with 0.5% and 1%CuO coated ZnO. (c) Raman spectra of ZnO with 3%, 5%, and 10% CuO coated ZnO. (d) Exploded view of the variation in the position of the E_2 (high) band for 0.5% and 1% CuO coated ZnO with reference to pure ZnO.

were examined by Field Emission Scanning Electron Microscope (JEOL JSM 6490-A).

The ability of CuO coated layers in suppressing the photocorrosion, compared to pure ZnO, under illumination, was evaluated by cyclic voltammetry (CV) using a VSP multichannel potentiostat (Biologic Science Instrument, USA) equipped with Ec-lab software in a three electrode system namely; glassy carbon electrode (working electrode), platinum (counter electrode) and Ag/AgCl saturated electrode (reference electrode). The powders, dispersed in chloroform, were coated at the tip of glassy carbon electrode by dropping 10 μL of suspension and dried in hot air for film formation. The homogeneity of the film was analyzed optically. For acquiring cyclic voltammograms under illumination, a 50 W halogen lamp was used as a light source. The cyclic voltammograms acquired for the coated samples, both in dark and under illumination, were compared with that of pure ZnO. All the measurements were carried out at room temperature (23 °C).

The photocatalytic activity of pure and CuO coated ZnO powders under sunlight exposure was performed by exposing 150 mL of 30 ppm of respective nitrophenol solution containing the optimized amount (150 mg) of respective catalyst in a Pyrex glass reactor. The dimensions of the glass reactor were 15.5 (diameter) x 2.5(height). The evaluated effective surface area of the reactor was 189 cm^2. All the experiments were performed under identical conditions without stirring. The adsorption−desorption equilibrium between the catalysts and substrates was established by stirring the samples in the dark for 30 min. The optimization of the CuO coating was performed by exposing all the synthesized catalysts to sunlight under identical experimental conditions. 4-nitrophenol was used as substrate for optimization. The amount of the catalysts was optimized for pure ZnO and kept constant for rational comparison. All the experiments were performed with 150 mg catalyst loading under sunlight illumination of $800 \pm 100 \times 10^2$ lx (21.4939° N, 39.2503° E) and fixed period of the daylight i.e. from 930 to 1500 h. The progress of degradation process was monitored by drawing the samples after every 30 min in the first 2 h and after 60 min in the last hour. The catalyst was removed by using 0.20 μm Whatman syringe filter. The collected samples were analyzed by high performance liquid chromatography (HPLC, SPD-20A, Shimadzu Corporation, Japan) using 60:40 Methanol−water mixture as solvent and c18 column. Based on peak response, a 254 nm was selected for analysis. Thermo scientific, USA, ion chromatograph, Dionex (ICS-5000 + EG Eluent Generator), was used to measure the released ions during photocatalytic process. TOC-VCPH total carbon analyzer supplied by Shimadzu Corporation, Japan, measured total Organic Carbon (TOC) of the samples. Blank experiments were performed to estimate the decrease in concentration of the substrates by direct photolysis.

3. RESULTS AND DISCUSSION

Figure 1a shows the comparison of the solid-state absorption spectra of pristine and CuO coated ZnO powders, where an enhanced absorption of the CuO coated powders in the visible region, compared to pure ZnO, was observable. In pristine ZnO, the principle absorption with the sharp absorption edge between 3.0 and 3.2 eV appears due to the transitions between the O^{2-} (2p) levels (valence band) to Zn^{2+} ($3d^{10} - 4s$) orbitals (conduction band). The coating of CuO at the surface of ZnO results in the formation of two closely spaced conduction bands formed by the sharing of surface O^- entities between Cu^{2+} and Zn^{2+} surface states. The probability of the transition of electrons to the individual components depends on the population density of each state. The lower energy transitions between O^{2-} (2p) and Cu^{2+} ($3d^9$) compared to that of O^{2-} (2p) and Zn^{2+} ($3d^{10} - 4s$) results in the enhanced absorption in the visible region. The magnitude of the absorption increases with the increase in the density of CuO surface coating. Additionally the role of d−d transitions between the closely spaced Zn^{2+} and Cu^{2+} states for enhanced absorption cannot be neglected. The graphical evaluation of the band edges of pure and the CuO coated ZnO powders extracted by plotting ($F(R)$

DOI: 10.1021/acsami.5b01273
ACS Appl. Mater. Interfaces 2015, 7, 8757−8769

$\times h\upsilon)^{1/2}$ versus $h\upsilon$, where $F(R)$ is the Kubelka–Munk transformation of %R values, is presented in Figure 1b–d. The evaluated bandgap value of ~3.20 eV for pristine ZnO was in accordance with the literature values.[26,27] A gradual red shift in the bandgap values was observed with the increasing CuO coating. Accordingly, the band edges of 0.5%, 1%, 3%, 5%, and 10%CuO@ZnO were shifted to ~3.1 eV, ~3 eV, ~2.95 eV, ~2.75 eV, and ~2.65 eV, respectively. The shifting of the bandgap energies to lower values may be regarded as the consequence of the enhanced combined transitions from O^{2-} (2p) to Zn^{2+} ($3d^{10}$ − 4s) and to Cu^{2+} ($3d^9$).

Figure 2a shows the comparison of PL spectra of pure and CuO@ZnO powders, where a significant decrease in the emission intensity of the characteristic bands of ZnO can be noticed. Pure ZnO is a highly florescent material with a number of emission bands. In this study, besides low intensity bands, the intense sharp band centered at ~389 nm and a broad band at ~495 nm were of particular interest from a surface modification point of view. The positions of these bands with minor variations were in accordance with the literature values.[17,27] The intense band at 389 nm (3.187 eV) epitomizes the de-excitations from the conduction band composed of Zn^{2+} (3d) to the valence band constituted by O^{2-} (2p) while the broad band ~495 nm represents the emissions due to excitations between Zn^{2+} and singly charged surface oxygen, respectively.[17,28] A significant decrease in the intensity of all the emission bands of ZnO to varying extent, with the increasing surface coating of CuO, depicted that the excited charges are trapped by the surface CuO states that resulted in the quenching of the emission. An average decrease of ~90% in the intensity of the band at 389 nm indicated that surface CuO successfully inhibits the electron–hole recombination process to prolong the lifetime of the excited state whereas the decreased intensity (~85%) of the broad band at 495 nm verified the engagement of singly charged surface oxygen by Cu^{2+} entities.

For clarity, the comparison of the Raman spectra of pristine and 0.5% and 1% CuO coated ZnO is presented in Figure 2b, while the comparison of pure ZnO with 3%, 5%, and 10% CuO coated ZnO is shown in Figure 2c. In the current study, the Raman active modes in pure ZnO appeared at 99.09 cm^{-1}, 331.95 cm^{-1}, 379.20 cm^{-1}, 437.50 cm^{-1}, 525.47 cm^{-1}, 575.40 cm^{-1}, and 1152.03 cm^{-1}. The observed values were in good agreement with the literature values.[29] Also the origin of these bands is already very well explained in the literature.[29] To evaluate the effect of increasing the CuO coating on the ZnO surface, we concentrated on the E_2 (high) band at 437.50 cm^{-1}, which is associated with the transitions of surface Zn–O^- groups.[35] As per our perception, the shift in the position and the increase or decrease in the intensity of the E_2 (high) band can reveal valuable information about the site of attachment of Cu^{2+} ions at the surface of ZnO, thus forming CuO after calcination. As presented in Figure 2b, compared to pure ZnO, a significant decrease in the intensity of E_2 (high) was observable for 0.5% and 1% CuO@ZnO, depicting that CuO forms the homogeneous surface layers by sharing the surface O^- entities. Additionally, the shifting of the E_2 (high) band toward higher energy, as presented in the exploded view (Figure 2d), revealed the CuO induced rigidity in the system. For 0.5% and 1% CuO coated ZnO, the E_2 (high) band is shifted to 435.62 and 433.68 cm^{-1}, respectively. With the increasing surface CuO coating, i.e. for 3% and beyond, as presented in Figure 2c, the bands due to surface CuO dominate the spectra and mask the bands of ZnO. The bands due to surface CuO appear at 199.37 cm^{-1}, 320.38 cm^{-1}, 429.30 cm^{-1}, 562.88 cm^{-1}, and 1115.87 cm^{-1}.

Figure 3 shows the comparison of the XRD patterns of pristine ZnO and CuO coated ZnO powders, where the

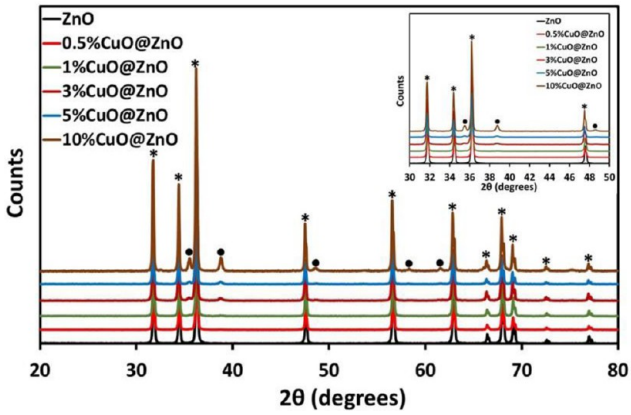

Figure 3. Comparison of the XRD patterns of ZnO with 0.5%, 1%, 3%, 5%, and 10%CuO coated ZnO from 2θ = 20° to 2θ = 80°. The reflections due to ZnO and CuO coating are marked by "∗" and "●" respectively. The inset shows the exploded view from 2θ = 30° to 2θ = 50°.

reflections due to ZnO are marked with "∗" while the reflections due to CuO coating are identified by "●". As observed in our previous communication,[17,18] the major reflections due to ZnO appearing at 2θ values of 31.7, 34.4, 36.2, 47.5, 56.5, 62.8, 67.9, and 69.05 were matching with hexagonal ZnO (JCPDS 36-1451). A noticeable decrease in the intensity of the above-mentioned reflections and the appearance of additional reflections at 2θ values of 35.6, 38.7, 48.6, 58.4, and 61.6 with the increasing surface CuO coating verified the presence of CuO. The intensity of the reflections due to CuO increased with the increasing CuO coating. The reflections were matched with monoclinic CuO (JCPDS 05-0661). These reflections are more prominent in the exploded view (2θ = 30° to 50°) presented in the inset of Figure 3. The absence of the reflections due to Cu or Cu_2O verified the formation of phase pure surface layers of CuO coating without any alteration in the oxidation state.

The comparison of the wide angle XPS survey scans of pure and CuO coated ZnO powders is presented in Figure 4a, where the peaks due to all the components such as Cu, Zn, and O are observable. The major peaks representing the core levels of the individual components are identified by dotted lines. Although the spectrum is dominated by the peaks due to ZnO base, however, the growth of Cu peaks with increasing CuO coating is noticeable. The C 1s reference peak at 284.6 eV is also observable in all the scans. The variation in the peak position of O 1s can furnish valuable information regarding the sites of attachments of Cu^{2+} and the change in the surface composition of ZnO after the formation of CuO under calcination. Compared to pure ZnO, the increased asymmetry and shifting in the O 1s peak positions was witnessed. To estimate the change in the surface oxygen environment with the increasing CuO coating, the O 1s profiles of pure ZnO and CuO@ZnO catalysts were fitted (Gaussian) and compared in Figure 4b. The O 1s peak for pure ZnO was observed at 531.4 eV. Interestingly, for all the CuO coated samples the O 1s peaks

DOI: 10.1021/acsami.5b01273
ACS Appl. Mater. Interfaces 2015, 7, 8757–8769

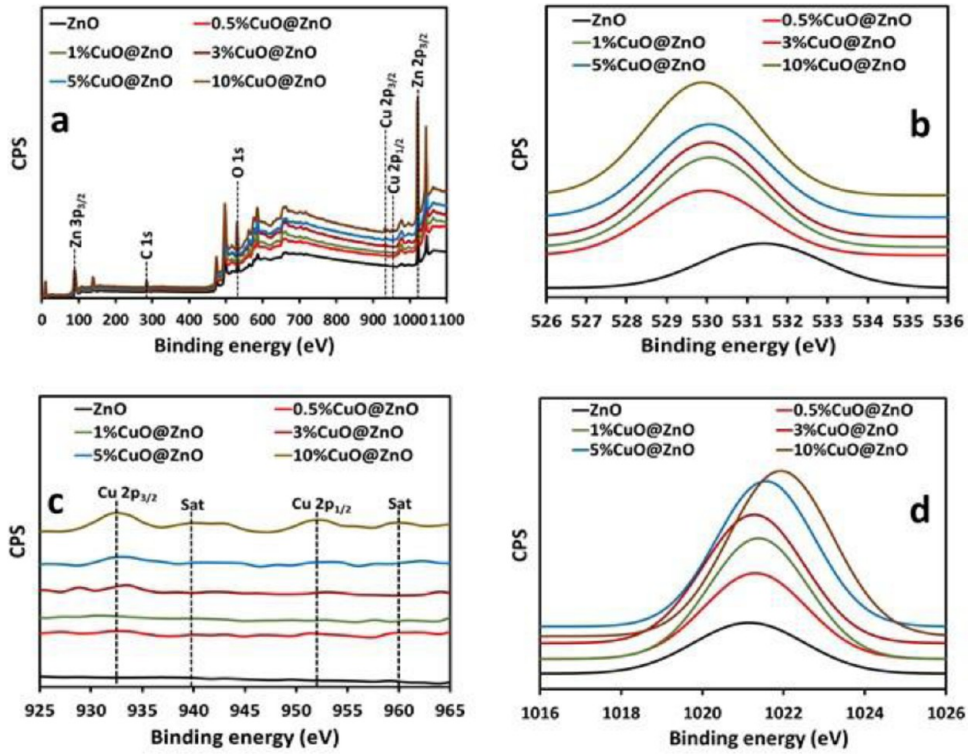

Figure 4. Comparison of (a) the XPS survey scan and (b) O 1s, (c) Cu 2p, and (d) Zn 2p peaks of pure ZnO with 0.5%, 1%, 3%, 5%, and 10% CuO coated ZnO catalysts. The survey scan was performed in the range of 0 to 1100 eV.

were shifted to lower binding energies. Till 5% CuO coating the observed values were 530.4 eV, while for 10% CuO coating the value was shifted to 529.9 eV. The shift in the binding energy of O 1s clearly depicted the changes in the oxygen environment at the surface due to CuO coating and verified that the incoming Cu^{2+} binds with the surface oxygen entities forming surface CuO. The significant shift of 1.5 eV, for 10% CuO@ZnO, also confirmed the majority surface coverage by CuO.

The comparison of the growth of the 2p spin−orbit splitted core levels of Cu, i.e. Cu $2p_{1/2}$ and Cu $2p_{3/2}$, with the increasing CuO coating is presented in Figure 4c. The Cu $2p_{1/2}$ and Cu $2p_{3/2}$ peaks were observed at ∼932.6 eV and ∼952.8 eV, respectively, which corresponds to Cu in the 2+ oxidation state.[30] Along with the spin−orbit splitted Cu 2p core levels, additional satellite peaks at ∼940 eV and ∼959.8 eV, characteristic of partially filled d-orbitals ($3d^9$ in this case of Cu^{2+}), were also noticed. It is important to mention here that due to the matrix effect of ZnO the Cu 2p splitted peaks were asymmetric in shape. Additionally, a minor shifting in the peak maxima was also observable because of the interaction between the CuO and ZnO; however, the observed values were well in accordance with the literature values for CuO, proving null variation in the oxidation state of Cu^{2+} during the coating process.[30] Moreover, the absence of the peaks due to Cu and Cu_2O also supported the findings.

For pure ZnO, the intense peaks at ∼89.0 eV, ∼1021.4 eV, and ∼1045.6 eV, assigned to the Zn $3p_{3/2}$, Zn $2p_{3/2}$, and Zn $2p_{1/2}$ levels, respectively, were in accordance with the literature values.[18,31] The comparison of the normalized single peak fitted Zn $2p_{3/2}$ peaks for the pure and CuO coated ZnO samples is presented in Figure 4d. The strong interaction between the CuO and ZnO, at higher coating levels, i.e. 5% and 10%, resulted in the minor shifting of the corresponding peak maxima to ∼1021.8 and 1022.3 eV, respectively.

The comparison of high resolution FESEM images of pure and CuO coated ZnO catalysts, at 120,000× magnification, is presented in Figure 5. Although a wide particle size distribution ranging from 10 to 100 nm was noticed for pure ZnO, however, ≥80% of the particles were in the 20−60 nm range. Additionally, the sharp hexagonal edges of the ZnO particles were also perceptible (Figure 5a). The careful analysis of Figure 5b−f revealed the homogeneous deposition of CuO at the surface of ZnO without the formation of individual CuO particles. A minor aggregation of ZnO particles at higher CuO coatings (5% and 10%) was observed that resulted in the apparent increase in particle size. Apart from the observations mentioned above, the only noticeable difference in the morphology of pure and CuO coated ZnO powders was the depletion of sharp margins of hexagonal edges with the increasing surface coating of CuO.

Pristine hexagonal ZnO is renowned for its instability under illumination. In the current study, the effectiveness of CuO coating in suppressing or eliminating the photocorrosion of ZnO, before being subject to actual degradation/mineralization experiments, was estimated by performing the cyclic voltammetric studies of pure and CuO coated ZnO powders in the dark and under illumination. The comparison of the cyclic voltammetric behavior of pure and 0.5%, 1% and 3% CuO coated ZnO samples in the dark is presented in Figure 6, whereas the inset of the same figure presents the electrochemical behavior under illumination. In the dark, ZnO shows a stable behavior and the redox peaks due to the formation of zincate ions under the influence of the applied potential are observable. The CuO layers effectively suppress the formation of zincate ions, and the redox peaks appearing due to the

DOI: 10.1021/acsami.5b01273
ACS Appl. Mater. Interfaces 2015, 7, 8757−8769

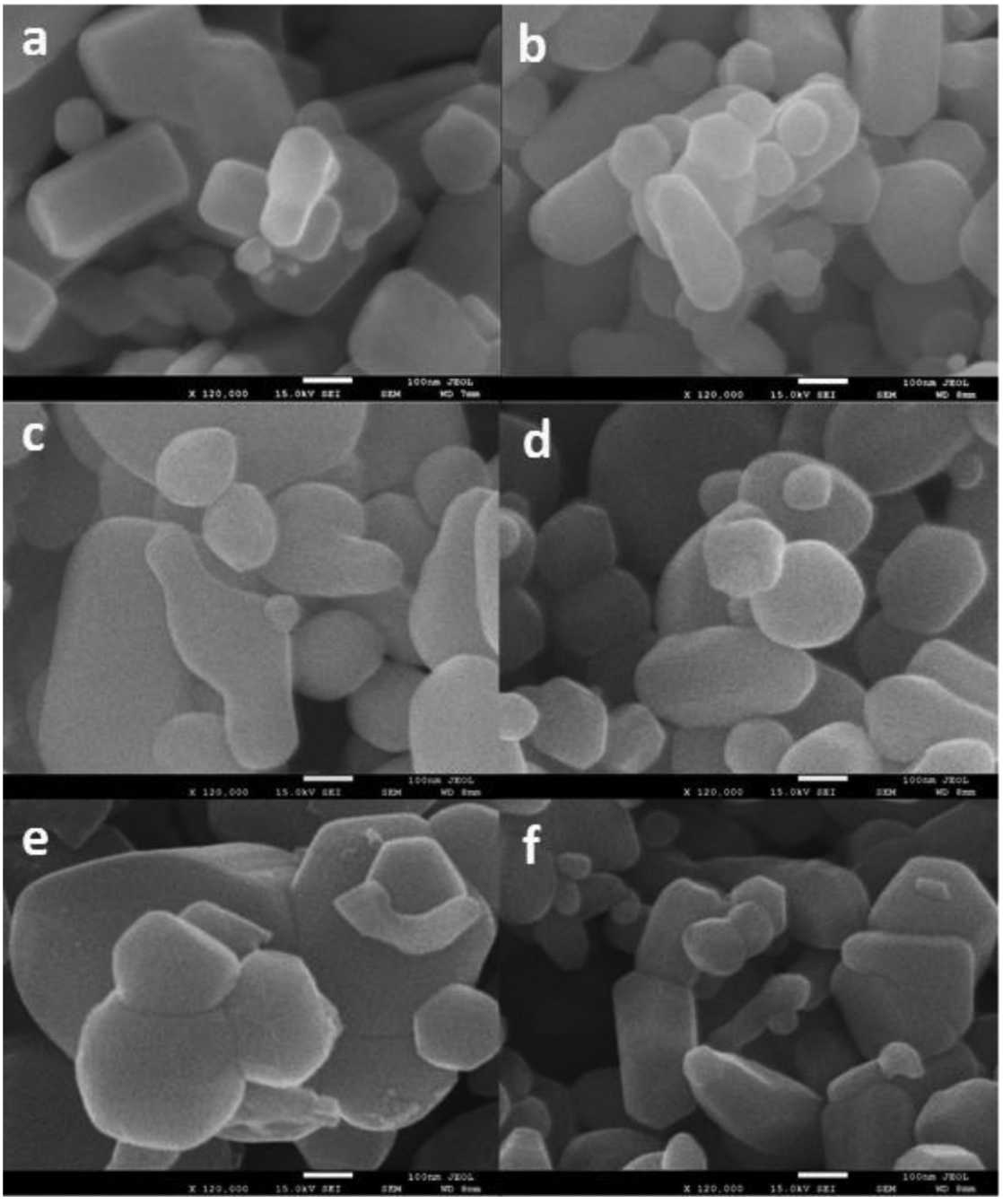

Figure 5. Comparison of high resolution (120,000×) FESEM images of (a) pure and (b) 0.5%, (c) 1%, (d) 3%, (e) 5%, and (f) 10% CuO coated ZnO, elaborating the homogeneous distribution of coated CuO at the surface of ZnO without altering its inherent hexagonal morphology.

formation of zincate ions are broadened for 0.5% and featureless for 1% and 3% CuO coated ZnO; however, additional peaks appeared for 3% CuO@ZnO, probably due to the formation of hydrated Cu^{2+} released from the surface. Under illumination, the additional peak at −1.04 V, for pure ZnO, marked by the circle in the inset of Figure 6, represents the photocorrosion of ZnO, i.e. anodic dissolution with the release of Zn^{2+} ions in the solution caused by the photoexcited entities. In the CV curves for CuO coated ZnO samples, the absence of the peak corresponding to the release of Zn^{2+} ions validated the effectiveness of coated CuO in eliminating the corrosion of ZnO by engaging the photon generated excited charge carriers. The anodic and cathodic dissolution processes that can be responsible for the release of Zn^{2+} ions in solution can be represented by the set of eqs 1−-3 below.

$$\mathrm{ZnO} + h\upsilon \xrightarrow{E>E_g} \mathrm{ZnO}(h_{vb}^{+} + e_{cb}^{-}) \quad (1)$$

$$\mathrm{ZnO} + 2h_{vb}^{+} + \mathrm{H_2O} \rightarrow \mathrm{Zn^{2+}(solution)} + \frac{1}{2}\mathrm{O_2(solution)} \quad (2)$$

$$\mathrm{ZnO} + 2e^{-} \rightarrow \mathrm{Zn^{2+}(solution)} + 2\mathrm{O^{-}(surface)} \quad (3)$$

Before the convulsion of actual photocatalytic experiments, as presented in Figure 7, the effect of the increasing surface density of CuO on ZnO was optimized for the degradation of 4-NP (30 ppm). It was noticed that, compared to ∼75%,

DOI: 10.1021/acsami.5b01273
ACS Appl. Mater. Interfaces 2015, 7, 8757−8769

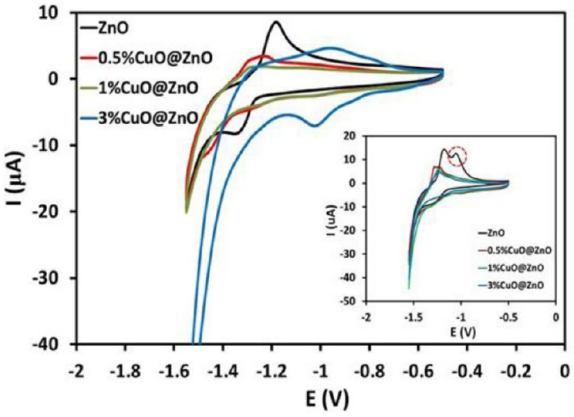

Figure 6. Comparison of the cyclic voltammetric behavior of pure and 0.5%, 1%, and 3% CuO coated ZnO in the dark. Inset: the same under illumination.

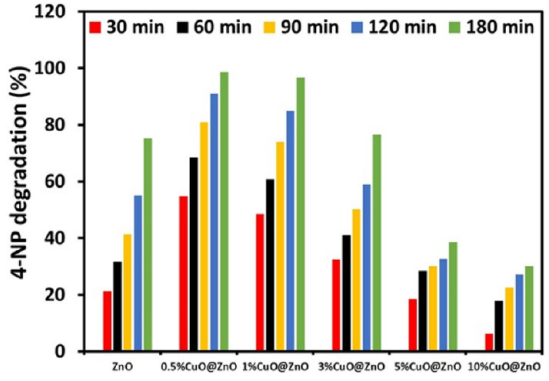

Figure 7. Optimization of CuO coating in comparison to pure ZnO for the maximum degradation of 4-NP (30 ppm) under sunlight exposure.

removal of 4-NP in 180 min of sunlight exposure for pure ZnO or 0.5%CuO coated ZnO degraded ~99% of the substrate in the same period. The activity of 1%CuO@ZnO (~96%) was higher than pure ZnO while that of 3% CuO@ZnO (~75%) was comparable with that of pure ZnO. In comparison with pure, a significantly lower activity was witnessed for 5% (~38%) and 10% (~30%) CuO coated ZnO catalysts. As discussed earlier that the increasing CuO layer density imparts better absorption of photons with the lowering of the bandgap (Figure 1a) as well, however, the decreased efficiency of the catalysts with increasing surface layer of CuO revealed that the increased spectral response does not essentially mean increased photocatalytic activity too. Additionally, it was also inferred that the increased absorption of photons, the existence of a bandgap in the visible region, and the suppression of the recombination process (Figure 1b) do not guarantee the efficient transfer of photoexcited charge carriers to reductants and oxidants for reactive oxygen species (ROS) generation that is regarded as an essential parameter for boosting the photocatalytic activity. It is also evident from the above-mentioned results that the lower CuO coatings (up to 1%) serve not only as the trapping sites for the photoexcited electrons but also efficiently transfer these to the dissolved/adsorbed O_2 for the generation of superoxide anion radicals ($O_2^{\bullet -}$), while on the other hand the trapping of excited electrons minimizes the possibility of electron−hole recombination, thus enhancing the yield of hydroxyl radicals ($^{\bullet}OH$) by holes initiated water-oxidation processes. The two processes are elaborated in eqs 4 and 5 below.

$$O_2(\text{adsorbed}) + e_{cb}^- \rightarrow O_2^{\bullet -} \quad (4)$$

$$H_2O + h_{vb}^+ \rightarrow {}^{\bullet}OH + H^+ \quad (5)$$

With the significant elevated activity imparted to ZnO by the lower concentrations of surface CuO, it can be visualized that surface Cu^{2+} species arrange in closely spaced surface states that facilitate the transition of excited electrons from Zn^{2+} ($3d^{10}$, $4s^0$) to Cu^{2+} ($3d^9$). As per our perception, this is only achievable by sharing the singly charges surface oxygen (O^-). Pictorially the same can be represented as in Scheme I.

Scheme I. Plausible Mechanism of Attachment of Cu^{2+} Ions at the Surface of ZnO To Form CuO

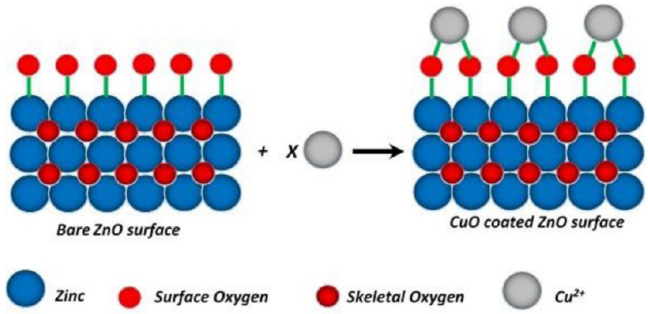

Based on the pictorial representation above (Scheme I) and the degradation results, it can be inferred that, at lower surface coating, the surface bonded Cu^{2+} species serve as trap centers for the photoexcited electron by sharing valence band with Zn^{2+} entities. The surface Cu^{2+} entities add an extra conduction band that augments the probability of the excited electron capture. The decreased emission intensity in the PL spectra also verified the same. Additionally, as the Zn^{2+} and Cu^{2+} entities are closely spaced, the lifetime of the excited states is further augmented by the inert transfer of electrons between the two states. The same can be represented pictorially as below in Scheme II.

With the increase in surface coating, the direct absorption of photons by surface CuO leads to a fair reduction in the direct

Scheme II. Proposed Mechanism of Excited Electron Trapping with a Low Concentration of CuO Present at the Surface of ZnO[a]

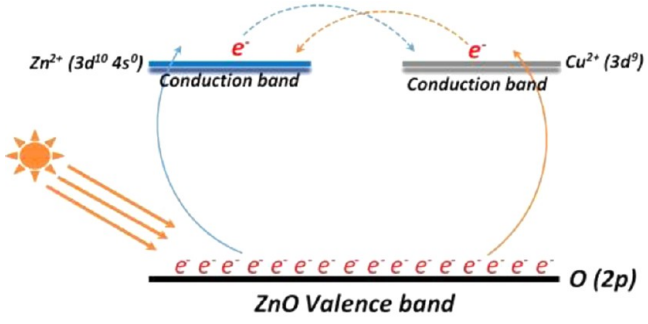

[a]The solid line shows the probability of direct transition from the O (2p) valence band to the Zn^{2+} ($3d^{10}$, $4s^0$) and Cu^{2+} ($3d^9$) conduction bands, whereas the dotted lines show the possibility of transitions between the Zn^{2+} and Cu^{2+} states for the prolonged lifetime of excited states.

DOI: 10.1021/acsami.5b01273
ACS Appl. Mater. Interfaces 2015, 7, 8757−8769

photon absorption by ZnO host. Zinc oxide is an n-type semiconductor with valence and conduction band edges at +2.89 V and −0.31 V, respectively, that demonstrates its ability for the generation of ROS (eqs 4 and 5), whereas CuO is a p-type semiconductor with the valence and conduction band edges at +1.25 V and +0.45 V, respectively.[34] The potential of the band edges predicts the inability of CuO to effectively contribute to the generation of ROS. At moderate CuO coating (3% and 5%), with the possibility of transfer of excited electrons from the conduction band of ZnO to that of CuO, an energetically allowed process, the extent of the generation of $O_2^{\bullet-}$ is drastically reduced. Additionally, the energetically favored transfer of h^+ from the valence band of ZnO to that of CuO affects the oxidation of adsorbed water, which results in the low yield of $^{\bullet}OH$ as well. At further higher CuO coating, i.e. 10%CuO@ZnO, with the possibility of the majority of sunlight photons directly absorbed by CuO coating, the occurrence of reverse processes, i.e. transfer of h^+ and e^- from CuO to ZnO, is energetically forbidden. As the superoxide anion radicals ($O_2^{\bullet-}$) are regarded as the major contributors in the degradation/mineralization process,[32,33] the consistent decrease in their production with the increasing CuO coating leads to decreased degradation/mineralization activity. The pictorial representation of the deactivating processes is given below in Scheme III.

Scheme III. Proposed Mechanisms of Deactivating Processes (a) at Moderate CuO Coating (3% and 5%), When the Photons Are Absorbed by the ZnO, a Fraction of Charge Carriers (e^- and h^+) Is Transferred to CuO, and (b) at Higher CuO Coating (10%), When the Majority Photons Is Absorbed by the CuO, De-excitation Is the Only Energetically Allowed Process

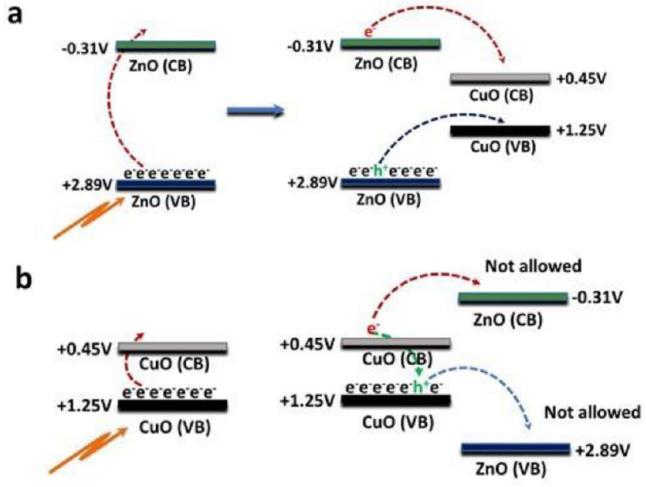

Based on the significantly higher degradation compared to pure and other CuO coated catalysts, the detailed investigation of photocatalytic degradation/mineralization of mono- and dinitrophenols was carried out over 0.5%CuO@ZnO under the exposure of the complete spectrum and the visible region of sunlight. The dark experiment revealed the low adsorption (7−9%) of MNP and DNP substrates. As MNPs and DNPs are weakly acidic substrates, compared to the pH of the water used, a mild decrease in the pH, ranging from 5.4 to 6.1, was noticed for 30 ppm of NPs substrate solutions. An increase in the pH of the suspension was observed with the addition of the catalyst or pure ZnO. It is important to mention here that, as per our perception, in an aqueous photocatalytic system, any change in the structure of the phenolic substrate as a result of the interaction with the photon generated ROS can be regarded as degradation. The loss of aromaticity or any substitution may shift the absorption maximum in the UV−visible analysis or shift the retention time in HPLC analysis. The time dependent HPLC chromatograms for the degradation of 2-NP, 3-NP, and 4-NP, in comparison to pure ZnO, are presented in Figure S1 (Supporting Information), whereas Figure 8a shows the comparison of the time-scale percentage degradation of 2-, 3-, and 4-NP over pure and 0.5% CuO coated ZnO extracted from the decrease in the concentration of the respective phenolic substrate. Compared to ∼19% degradation over pure ZnO, the 0.5% CuO coated catalyst degraded ∼80% of 2-NP in the initial 30 min of complete spectrum sunlight exposure, whereas compared to ∼30% and ∼21% degradation over ZnO, ∼43% and ∼55% of 3-NP and 4-NP was degraded in the same period, respectively. In 90 min of exposure, the removal of ≥99%, ≥80%, and 85% was observable for 2-NP, 3-NP, and 4-NP, respectively, whereas the degradation of these substrates was ≤65% for 2-NP and ≤50% for 3-NP and 4-NP over pure ZnO. 2-NP was completely degraded in 120 min of sunlight exposure while ≥90% of 3-NP and 4-NP was removed in the same period. For pure ZnO, a maximum degradation of ∼90% was noticed for 2-NP while for the other substrates (3-NP and 4-NP), it was less than ∼83%. The rates of degradation of the phenolic substrates were evaluated by applying the Langmuir−Hinshelwood kinetic model for pseudo first order reactions. The graphical evaluation of the rate constants "k" is presented in Figure 8b. The maximum rate of 0.050 min^{-1} was perceived for the degradation of 2-NP over 0.5% CuO@ZnO, whereas 0.020 min^{-1} and 0.019 min^{-1} was noticed for 4-NP and 3-NP, respectively. The observed rates of degradation of 2-, 3-, and 4NP over pure ZnO were 0.0120 min^{-1}, 0.007 min^{-1}, and 0.009 min^{-1}, respectively. Based on the percentage and rates of degradation, the order of degradation of mononitrophenols appeared as 2-NP > 4-NP > 3-NP. The simultaneous blank experiments revealed no significant change in the concentration of MNP substrates after 180 min of exposure.

The degradation of a substrate does not actually mean its complete removal. In the photocatalytic system, as discussed earlier, the interaction of ROS with the substrate may result in the formation of more hazardous off-shoots. Therefore, TOC removal (mineralization) efficiency of a catalyst is the actual measure of its suitability for the complete removal of substrates as well as intermediates. The comparison of the time-scale TOC removal of MNP isomers in the presence of pure and 0.5% CuO@ZnO is presented in Figure 8c. The comparison of Figure 8a and 8c revealed lower extent of TOC removal compared to degradation. Compared to ∼90% degradation of 2-NP in the initial 30 min of exposure, ∼40% of TOC was removed. The same was true for the other substrates as well; however, the TOC removal by 0.5% CuO@ZnO was much higher than the pure ZnO. A pattern similar to that of degradation was also witnessed for TOC removal as well. A maximum TOC removal of ∼93% was noticed for 2-NP, whereas, for 4-NP, it was ∼83% and ∼80% for 3-NP for the exposure of 180 min. As presented in Figure 8d, a trend similar to that of degradation was noticed in the rate of TOC removal. The evaluated rates of mineralization of 2-, 3- and 4-NP over 0.5% CuO@ZnO were 0.145 min^{-1}, 0.009 min^{-1}, and 0.010 min^{-1}, respectively, and significantly lower than the rates of

DOI: 10.1021/acsami.5b01273
ACS Appl. Mater. Interfaces 2015, 7, 8757−8769

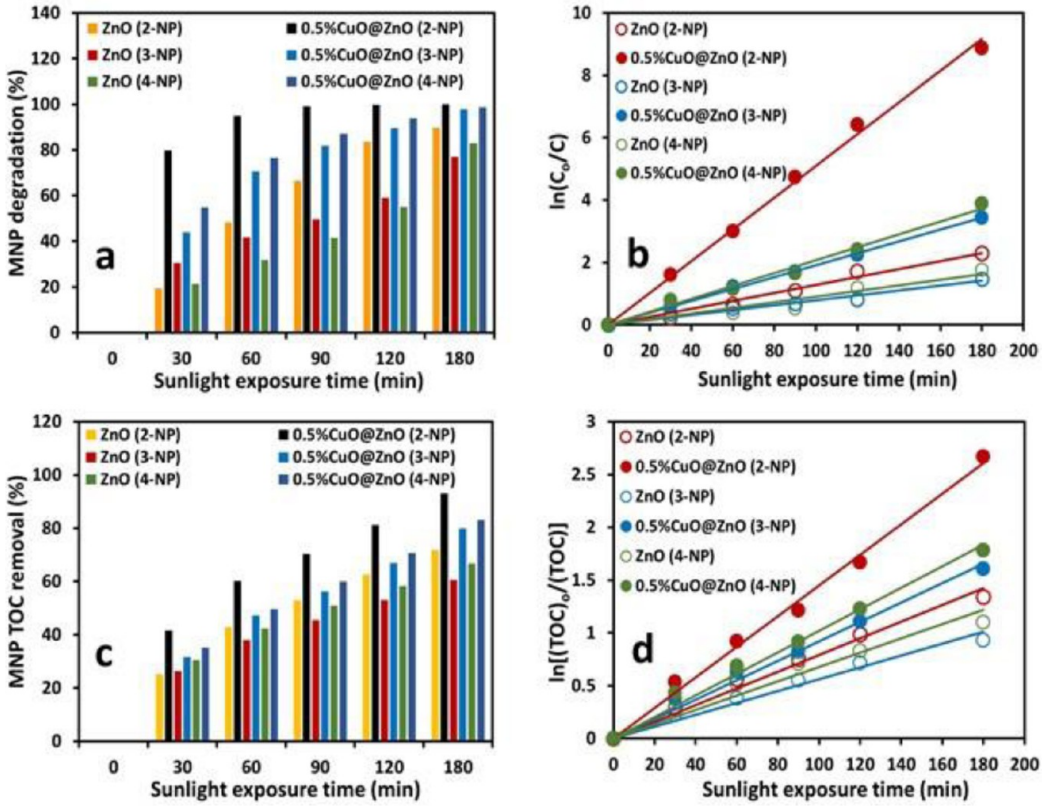

Figure 8. Comparison of (a) percentage degradation, (b) graphical evaluation of rate of degradation, (c) TOC removal, and (d) rate of TOC removal of 2-, 3-, and 4-NP (30 ppm each) over pure and 0.5% CuO coated ZnO under sunlight exposure.

degradation for the respective substrates. With these observations it might be inferred that the mineralization of MNP is not a single step process but rather proceeds through the formation of intermediates. The intermediates were further interacted by ROS to smaller fragments and then to mineralization finally.

The release of NO_2^- and NO_3^- ions during the degradation process was measured by ion chromatography (IC). The time-scale IC profiles for the release of these ions are presented in Figure S2 (Supporting Information). It was noticed that NO_2^- are the primary ions that are released as a consequence of ROS interaction and transformed into secondary anions by the further interaction of either ROS or the photon induced charge carriers such as "holes". It is important to mention here that due to the enhanced detector response for NO_3^-, the peaks due to NO_2^- ions are suppressed; therefore, based on the peak intensity, the comparison of NO_2^- ions released during the MNP degradation process was plotted as a function of sunlight exposure time and presented in Figure 9, while the inset of the same shows the comparison of the release of NO_3^- ions. The instantaneous release of NO_2^- ions revealed that the NO_2 groups bearing carbons of MNP are primary interaction sites for ROS. Additionally, the release of NO_2^- ions predicts the charged nature of ROS involved rather than neutral. The rapid degradation and mineralization of MNP also supports the involvement of superoxide anion radicals in both the processes. The charge separation induced by the presence of electronegative oxygen imposes the partial positive charge on the attached carbon atom that serves as a potential source of interaction with superoxide anions. The $O_2^{\bullet-}$ ions displace the nitro groups as nitrite ions and inserted themselves in the chain, causing the ring opening and formation of intermediates. The presence of a variety of oxygenated intermediates (formic acid,

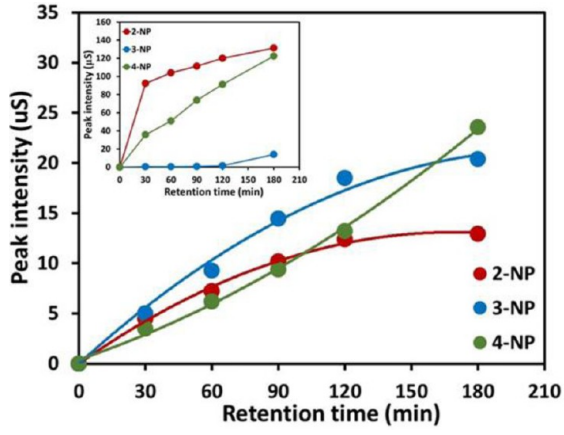

Figure 9. Comparison of the release of NO_2^- ions during the degradation of 2-, 3-, and 4-NP (30 ppm each) over pure and 0.5% CuO coated ZnO under sunlight exposure. The inset shows the comparison of the conversion of released NO_2^- to NO_3^- ions.

acetic acid, aliphatic alcohols, and esters) also supports this assumption. The difference in the rate of degradation is explainable on the basis of the extent of the position regulated charge separation induced by the nitro groups on the attached carbon. The rapid degradation of 2-NP is facilitated by the intramolecular hydrogen bonding that induces additional charge distortion. The intermolecular hydrogen bonding in 4-nitrophenol is an additional factor besides the inductive effect that facilitates its degradation. The absence of hydrogen bonding in 3-NP results in lower degradation of 3-NP. Additionally, the position and orientation of NO_2 groups in

DOI: 10.1021/acsami.5b01273
ACS Appl. Mater. Interfaces 2015, 7, 8757–8769

MNP also affect their rate of degradation. The other factors, based on the stability consideration that can influence the interaction of ROS with MNP isomers, are discussed in detail in our previous communication.[18]

The HPLC degradation profiles of dinitrophenol isomers, namely 2,4-, 2,5-, and 2,6-DNP, are presented in Figure S3 (Supporting Information) while the time-scale percentage degradation profiles evaluated on the basis of peak heights, in comparison to pure ZnO, are presented in Figure 10a. In the

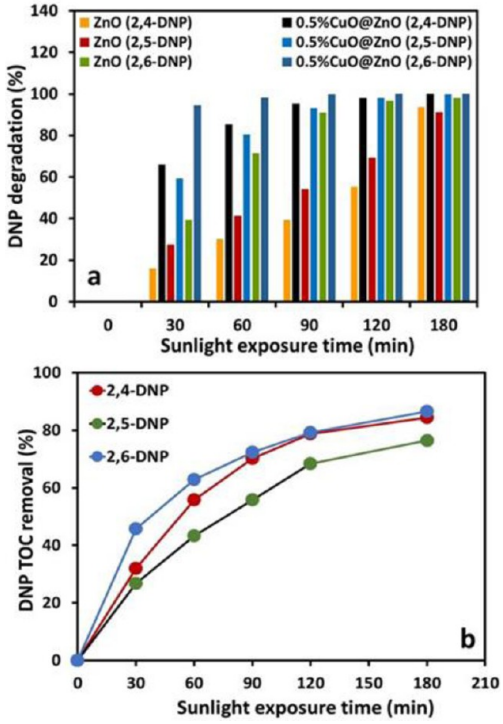

Figure 10. Comparison of (a) the degradation of 2,4-DNP, 2,5-DNP, and 2,6-DNP (30 ppm each) over pure and 0.5% CuO coated ZnO under sunlight exposure. (b) Percentage mineralization of 2,4-DNP, 2,5-DNP, and 2,6-DNP over 0.5% CuO coated ZnO.

presence of 0.5%CuO@ZnO, the degradation of all the DNP isomers was significantly higher than that of pure ZnO. Compared to ~66% and ~59% removal of 2,4- and 2,5-DNP, respectively, ~95% of 2,6-DNP was removed in 30 min of complete spectrum sunlight exposure. All the three substrates were completely removed in 180 min of sunlight exposure. Although a significantly higher degradation (~90%) of all the three substrates was noticed in the presence of pure ZnO in the same period, however, none of the isomer was completely removed. The graphical evaluation of the rate constants "k" for the degradation of DNP evaluated by plotting $\ln(C_o/C)$ versus the sunlight exposure time "t" is presented in Figure S4 (Supporting Information), where a rapid degradation of 2,6-DNP, at the rate of 0.068 min^{-1}, was calculated. The rates of degradation of 2,4- and 2,5-DNP were 0.040 min^{-1} and 0.032 min^{-1}, respectively. The comparison of the mineralization of DNP isomers under identical conditions to that of degradation is presented in Figure 10b. Compared to the mineralization of ~75% for 2,5-DNP, the mineralization of >85% for 2,4- and 2,6-DNP isomers was noticed. Among all the DNP isomers the degradation as well as mineralization of 2,6-DNP was significantly higher. Based on the removal and mineralization rates, the order of degradation of DNP isomers appeared as 2,6-DNP > 2,4-DNP >2,5-DNP. Similar to MNP degradation, no degradation of DNP isomers was observed as a result of direct photolysis after 180 min of exposure.

Based on the above-mentioned statistics, it was inferred that the position of nitro groups regulates their degradation. The rapid degradation of 2,6-DNP is attributed to the enhanced magnitude of hydrogen bonding due to the presence of nitro groups at the positions adjacent to phenolic carbon that imparts partial positive character at the 2- and 6-position, thus generating additional sites for $O_2^{\bullet-}$ ions interaction. For 2,4-DNP, the hydrogen bonding of the NO_2 group at the 2-position and the enhanced −I effect by the NO_2 group at the 4-position results in the distortion of the electronic cloud, which facilitates the degradation process. Although the NO_2 group at the 2-position undergo hydrogen bonding in 2,5-DNP, however, the inductive effect of the NO_2 group present at the 5-position is not effective enough to induce substantial polarity for $O_2^{\bullet-}$ ions interaction.

The comparison of the percentage degradation and mineralization of MNP and DNP isomers is presented in Figure 11a and its inset, respectively. Compared to the MNP

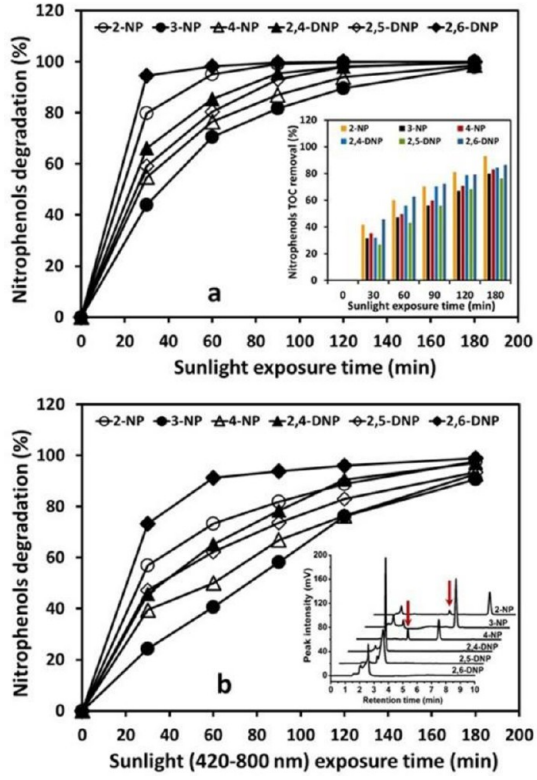

Figure 11. Comparison of the degradation of MNP and DNP isomers (30 ppm each) over 0.5% CuO coated ZnO under (a) sunlight or (b) visible light (420−800 nm) exposure. The inset of (a) shows the comparison of mineralization of the above-mentioned substrates under sunlight exposure, whereas the inset of (b) shows the HPLC profiles after 30 min of sunlight (420−800 nm).

degradation, a higher degradation was noticed for DNP isomers. This observation is explainable on the basis of the fact that, compared to MNP, the DNP isomer has the advantage of an additional reactive site that enhances the degradation. On the other hand, the mineralization of MNP isomers was significantly faster than that of DNP isomers. In the degradation of DNP isomers, as the number of ROS

DOI: 10.1021/acsami.5b01273
ACS Appl. Mater. Interfaces 2015, 7, 8757−8769

generated under identical conditions remains constant in the aqueous fixed-bed experiments, the majority of ROS that are produced are consumed in the degradation process and a few are available for mineralization. The rate of mineralization of DNP isomers increases with the decrease in the concentration of the original substrate. In a simple analogy, the degradation of DNP isomers requires twice the number of ROS as compared to MNP isomers. The low degradation of 3-NP and 2,5-DNP predicts the importance of orientation and position of NO_2 group(s) in the degradation of nitrophenols. The overall combined order of degradation over 0.5%CuO@ZnO after 30 min of sunlight exposure appeared as follows:

2,6-DNP > 2-NP > 2,4-DNP > 2,5-DNP > 4-NP > 3-NP

The activity of 0.5%CuO@ZnO toward MNP and DNP isomers was also evaluated in the visible region (420−800 nm) of the solar spectrum. The comparison of the percentage degradation in the visible region (420−800 nm) of all the phenolic substrates, MNP and DNP isomers, is presented in Figure 11b. The catalyst showed excellent activity for the degradation of all the substrates in the visible region of the solar spectrum. Although slightly lower than the exposure in the complete spectrum of sunlight, it is, however, significantly higher than the pure ZnO. This observation revealed that although not much lowering in the bandgap was witnessed for 0.5%CuO@ZnO a marked change in the shifting of the absorption cross section in the visible region of the spectrum, as presented in Figure 1a, was noticed. The extended absorption cross section and the presence of 0.5% CuO as trapping and transfer agent, PL analysis (Figure 2a), at the surface resulted in the enhanced degradation. Additionally, the assumption of sharing of the valence band by Cu^{2+} sounds valuable in this context. A similar observation was noticed in the mineralization process. No change in the order of degradation or mineralization of MNP and DNP isomers was observable.

Recently, a limited role of hydroxyl radicals ($OH^{\bullet}$) has been proposed rather than the generation of hydroxyl radicals being negated in the aqueous phase photocatalytic processes and a complex route has been proposed. Additionally, the survival and the reactivity of the hydroxyl radicals ($OH^{\bullet}$) have been associated with the pH of the system.[25,32,33] In the current study, in complete spectrum sunlight exposure, the absence of aromatic hydroxyl group substituted intermediates, in the GC-MS analysis of selected samples, further strengthened the view of minor or near absence role of hydroxyl radicals in the degradation process. However, in the exposure of the visible region of the sunlight, an interesting change in terms of intermediate formation was noticed. The HPLC profiles of MNP and DNP isomers after 30 min of visible region of sunlight exposure are presented in the inset of Figure 11b. Except for 2- and 4-NP, the positions (retention times) of the intermediates formed in the visible light exposure were similar to those observed under sunlight exposure (Figure S1, Supporting Information). In the HPLC degradation profiles of 2- and 4-NP, the additional peaks, marked by red arrows, at 5.25 and 3.55 min, respectively, were noticeable. An initial increase until 90 min of exposure followed by a decrease in the peak intensity afterward was observable. The GC chromatograms obtained in the identification of these intermediates are presented in Figure 12, where apparently no difference in the retention time of the intermediates was observed in HPLC;

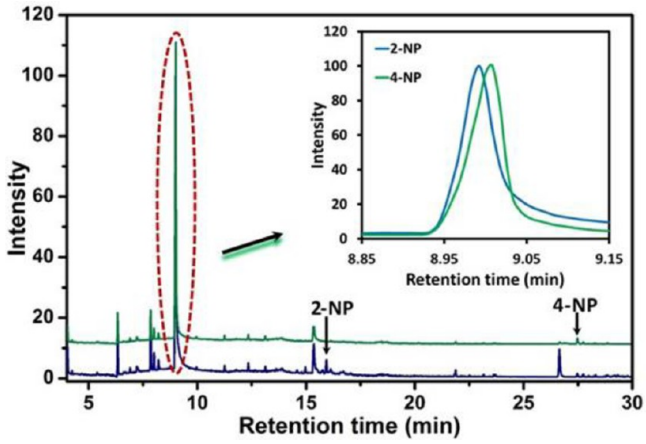

Figure 12. Comparison of the GC profiles of 2-NP and 4-NP over 0.5% CuO coated ZnO under sunlight (420−800 nm) exposure. Inset: exploded view to verify the difference in the retention time of apparently the same products.

however, the exploded view, as presented in the inset of Figure 12, revealed a shift in the retention time of both. The GC-MS library peak search and match analysis revealed that both have the same molecular formula ($C_8H_9NO_2$) with the mass number 151 g/mol, which led to the speculation that both the peaks are due to isomers of the same compound formed by the interaction of either ROS or the reactive intermediates with the NO_2 groups of 2- and 4-NP. It may also be inferred that these products are also formed in the complete spectrum sunlight exposure but are, however, degraded immediately after their formation due to the increased formation of ROS, mainly $O_2^{\bullet-}$, under the influence of UV photons.

As monitored by ICP, the release of Zn^{2+} and Cu^{2+} ions for 0.5% and 1% CuO@ZnO was negligible, i.e. <1 ppm after 180 min of exposure, while for pure ZnO the concentration of Zn^{2+} ions in the solution was ∼17 ppm in the same period of complete spectrum sunlight exposure. Although no release of Zn^{2+} ions was noticed for 5% and 10% CuO@ZnO, however Cu^{2+} ions in the solution were detected at a noticeable concentration. The total concentration of Cu^{2+} detected for 5% and 10% CuO@ZnO catalysts by ICPE-9000 was 1.9 and 3.4 ppm, respectively, after 180 min of sunlight exposure, whereas, in the visible region (420−800 nm) exposure, the measured concentration was well below 1 ppm. These findings validated the observations of pre-exposure cyclic voltammetric analysis.

As presented in Figure S5 (Supporting Information), the 0.5% CuO@ZnO catalyst showed sustained activity, without any significant decrease in the activity, in three cycles estimated by the repeated exposures after 24 h and 48 h by replacing the fresh substrate (2-NP) under identical experimental conditions.

4. CONCLUSIONS

The study revealed that the CuO surface coating of ZnO did the following:

- improved the spectral response of ZnO in the visible region
- effectively suppressed the $e^{-}-h^{+}$ recombination process
- enhanced the photocatalytic activity of ZnO in both the visible and complete spectrum sunlight exposure
- effectively suppressed the photocorrosion of ZnO

The other silent features of the study are as follows:

DOI: 10.1021/acsami.5b01273
ACS Appl. Mater. Interfaces 2015, 7, 8757−8769

- The degradation process proceeds with ring opening and release of NO_2^- ions.
- NO_2^- ions are further oxidized to NO_3^- ions.
- The lower CuO coatings enhanced the photocatalytic degradation/mineralization process while the higher coatings were detrimental.
- Superoxide anion radicals were identified as major oxidants; however, the existence of hydroxyl radicals cannot be neglected.
- Superoxide anion radicals interact simultaneously with the substrates as well as intermediates.

■ ASSOCIATED CONTENT

Supporting Information

HPLC profiles for the degradation of MNP (Figure S1) and DNP (Figure S3) isomers in comparison to pure ZnO. The IC profiles for the release of NO_2^- and NO_3^- (Figure S2), graphical evaluation of the rate constant for the degradation of DNP (Figure S4), and comparison of the catalyst recyclability (Figure S5). This material is available free of charge via the Internet at http://pubs.acs.org/.

■ AUTHOR INFORMATION

Corresponding Author

* E-mail: afmuhammad@kau.edu.sa, hameedch@yahoo.com Tel: +966-12-6402000/25284. Fax: +966-12-6952674.

Notes

The authors declare no competing financial interest.

■ ACKNOWLEDGMENTS

A.H., M.A., M.T.Q., and I.M.I.I. are thankful to the Center of Excellence in Environmental Studies (CEES); Chemistry Department, Faculty of Science, King Abdulaziz University, and Ministry of Higher Education (MoHE), KSA, for support.

■ REFERENCES

(1) Hoffmann, M. R.; Martin, S. T.; Choi, W.; Bahnemann, D. W. Environmental Applications of Semiconductor Photocatalysis. *Chem. Rev.* **1995**, *95*, 69−96.

(2) Ollis, D. F., Al-Ekabi, H., Eds. *Photocatalytic Purification and Treatment of Water and Air*; Elsevier: Amsterdam, 1993.

(3) Serpone, N., Pelizzetti, E., Eds. *Photocatalysis, Fundamentals and Applications*; Wiley: New York, 1989.

(4) Guillard, C.; Disdier, J.; Herrmann, J. M.; Lehaut, C.; Chopin, T.; Malato, S.; Blanco, J. Comparison of Various Titania Samples of Industrial Origin in the Solar Photocatalytic Detoxification of Water Containing 4-Chlorophenol. *Catal. Today* **1999**, *54*, 217−228.

(5) Gaya, U. I.; Abdullah, A. H. Heterogeneous Photocatalytic Degradation of Organic Contaminants over Titanium Dioxide: A Review of Fundamentals, Progress and Problems. *J. Photochem. Photobiol. C* **2008**, *9*, 1−12.

(6) Tanaka, K.; Luesaiwong, W.; Hisanaga, T. Photocatalytic Degradation of Mono-, Di- and Trinitrophenol in Aqueous TiO_2 Suspension. *J. Mol. Catal. A: Chem.* **1997**, *122*, 67−74.

(7) Linsebigler, A. L.; Lu, G. Q.; Yates, J. T. Photocatalysis on TiO_2 Surfaces: Principles, Mechanisms, and Selected Results. *Chem. Rev.* **1995**, *95*, 735−758.

(8) Esplugas, S.; Giménez, J.; Conteras, S.; Pascual, E.; Rodríguez, M. Comparison of Different Advanced Oxidation Processes for Phenol Degradation. *Water Res.* **2002**, *36*, 1034−1042.

(9) Pera-Titus, M.; Garcia-Molina, V.; Bañ os, M. A.; Giménez, J.; Esplugas, S. Degradation of Chlorophenols by Means of Advanced Oxidation Processes: A General Review. *Appl. Catal., B* **2004**, *47*, 219−256.

(10) Kumar, S. G.; Koteswara Rao, K. S. R. Zinc Oxide Based Photocatalysis: Tailoring Surface-Bulk Structure and Related Interfacial Charge Carrier Dynamics for Better Environmental Applications. *RSC Adv.* **2015**, *5*, 3306−3351.

(11) Schneider, J.; Matsuoka, M.; Takeuchi, M.; Zhang, J.; Horiuchi, Y.; Anpo, M.; Bahnemann, D. W. Understanding TiO_2 Photocatalysis: Mechanisms and Materials. *Chem. Rev.* **2014**, *114*, 9919−9986.

(12) Chong, M. N.; Bo Jin, B.; Chow, C. W. K.; Saint, C. Recent Developments in Photocatalytic Water Treatment Technology: A Review. *Water Res.* **2010**, *44*, 2997−3027.

(13) Aslam, M.; Ismail, I. M. I.; Salah, N.; Chandrasekaran, S.; Qamar, M. T.; Hameed, A. Evaluation of Sunlight Induced Structural Changes and Their Effect on the Photocatalytic Activity of V_2O_5 for the Degradation of Phenols. *J. Hazard. Mater.* **2014**, *286C*, 127−135.

(14) Hameed, A.; Aslam, M.; Ismail, I. M. I.; Salah, N.; Fornasiero, P. Sunlight Induced Formation of Surface Bi_2O_{4-x}−Bi_2O_3 Nanocomposite during the Photocatalytic Mineralization of 2-Chloro and 2-Nitrophenol. *Appl. Catal., B* **2015**, *163*, 444−451.

(15) Aslam, M.; Ismail, I. M. I.; Chandrasekaran, S.; Hameed, A. Morphology Controlled Bulk Synthesis of Disc-Shaped WO_3 Powder and Evaluation of its Photocatalytic Activity for the Degradation of Phenols. *J. Hazard. Mater.* **2014**, *276*, 120−128.

(16) Zhao, Q.; Ju, D.; Deng, X.; Huang, J.; Cao, B.; Xu, X. Morphology-Modulation of SnO_2 Hierarchical Architectures by Zn Doping for Glycol Gas Sensing and Photocatalytic Applications. *Sci. Rep.* **2015**, *5*, 7874.

(17) Aslam, M.; Ismail, I. M. I.; Almeelbi, T.; Salah, N.; Chandrasekaran, S.; Hameed, A. Enhanced Photocatalytic Activity of V_2O_5−ZnO Composites for the Mineralization of Nitrophenols. *Chemosphere* **2014**, *117*, 115−123.

(18) Hameed, A.; Aslam, M.; Ismail, I. M. I.; Chandrasekaran, S.; Kadi, M. W.; Gondal, M. A. Sunlight Assisted Photocatalytic Mineralization of Nitrophenol Isomers over W^{6+} Impregnated ZnO. *Appl. Catal., B* **2014**, *160*−*161*, 227−239.

(19) Aslam, M.; Ismail, I. M. I.; Chandrasekaran, S.; Almeelbi, T.; Hameed, A. The Suitability of Ce^{3+}-Modified ZnO Photocatalyst for the Mineralization of Monochlorophenol Isomers in Sunlight Exposure. *RSC Adv.* **2014**, *4*, 49347−49359.

(20) Ismail, I. M. I.; Aslam, M.; Almeelbi, T.; Chandrasekaran, S.; Hameed, A. Ce^{3+} Impregnated ZnO: A Highly Efficient Photocatalyst for Sunlight Mediated Mineralization. *RSC Adv.* **2014**, *4*, 16043−16046.

(21) Mageshwari, K.; Sathyamoorthy, R. Flower-shaped CuO Nanostructures: Synthesis, Characterization and Antimicrobial Activity. *J. Mater. Sci. Technol.* **2013**, *29*, 909−914.

(22) Princea, J.; Tzompantzib, F.; Mendoza-Damiánb, G.; Hernandez-Beltranc, F.; Valentec, J. S. Photocatalytic Degradation of Phenol by Semiconducting Mixed Oxides Derived from Zn(Ga)Al Layered Double Hydroxides. *Appl. Catal., B* **2015**, *163*, 352−360.

(23) Wang, K. H.; Hsieh, Y. H.; Chen, L. J. The Heterogeneous Photocatalytic Degradation, Intermediates and Mineralization for the Aqueous Solution of Cresols and Nitrophenols. *J. Hazard. Mater.* **1998**, *59*, 251−260.

(24) Teh, C. M.; Mohamed, A. R. Roles of Titanium Dioxide and Ion-Doped Titanium Dioxide on Photocatalytic Degradation of Organic Pollutants (Phenolic Compounds and Dyes) in Aqueous Solutions: A Review. *J. Alloys Compd.* **2011**, *509*, 1648−1660.

(25) Paola, A. D.; Marci, G.; Palmisano, L.; Schiavello, M.; Uosaki, K.; Ikeda, S.; Ohtani, B. Preparation of Polycrystalline TiO_2 Photocatalysts Impregnated with Various Transition Metal Ions: Characterization and Photocatalytic Activity for the Degradation of 4-Nitrophenol. *J. Phys. Chem. B* **2002**, *106*, 637−645.

(26) Jayabharathi, J.; Sundharesan, M.; Prabhakaran, A.; Karunakaran, C. Understanding the Binding Interaction of Imidazole with ZnO Nanomaterials and Clusters of Imidazole with ZnO Nanomaterials and Clusters. *RSC Adv.* **2015**, *5*, 9518−9531.

(27) Srikant, V.; Clarke, D. R. On the Optical Band gap of Zinc Oxide. *J. Appl. Phys.* **1998**, *83*, 5447.

DOI: 10.1021/acsami.5b01273
ACS Appl. Mater. Interfaces 2015, 7, 8757−8769

(28) Willander, M.; Nur, O.; Sadaf, J. R.; Qadir, M. I.; Zaman, S.; Zainelabdin, A.; Bano, N.; Hussain, I. Luminescence from Zinc Oxide Nanostructures and Polymers and Their Hybrid Devices. *Materials* **2010**, *3*, 2643−2667.
(29) Cuscó, R.; Alarcón-Lladó, E.; Ibáñez, J.; Artús, L.; Jiménez, J.; Wang, B.; Callahan, M. J. Temperature Dependence of Raman Scattering in ZnO. *Phys. Rev. B: Condense Matter Mater. Phys.* **2007**, *75*, 165202.
(30) *NIST X-ray Photoelectron Spectroscopy Database, SRD 20*, Version 3.5; National Institute of Standards and Technology: Gaithersburg, MD, 2008.
(31) Mai, N. T.; Thuy, T. T.; Mott, D. M.; Maenosono, S. Chemical Synthesis of Blue-Emitting Metallic Zinc Nano-Hexagons. *CrystEngComm* **2013**, *15*, 6606−6610.
(32) Lathasree, S.; Nageswara Rao, A.; Siva Sankar, B.; Sadasivam, V.; Rengaraj, K. Heterogeneous Photocatalytic Mineralization of Phenols in Aqueous Solutions. *J. Mol. Catal. A: Chem.* **2004**, *223*, 101−105.
(33) Ahmed, S.; Rasul, M. G.; Martens, W. N.; Brown, R. J.; Hashib, M. A. Heterogeneous Photocatalytic Degradation of Phenols in Wastewater: A Review on Current Status and Developments. *Desalination* **2010**, *261*, 3−18.
(34) Xu, S.; Qin, Y.; Xu, C.; Wei, Y. G.; Yang, R.; Wang, Z. L. Self-Powered Nanowire Devices. *Nat. Nanotechnol.* **2010**, *5*, 366−373.
(35) Panda, S. K.; Jacob, C. Surface enhanced Raman scattering and photoluminescence properties of catalytic grown ZnO nanostructures. *Appl. Phys. A* **2009**, *96*, 805−811.

DOI: 10.1021/acsami.5b01273
ACS Appl. Mater. Interfaces 2015, 7, 8757−8769